Available online at www.sciencedirect.com

SciVerse ScienceDirect

Ceramics International 39 (2013) S437–S440

CERAMICS INTERNATIONAL

www.elsevier.com/locate/ceramint

Fabrication of well-crystallized mesoporous ZrO_2 thin films via Pluronic P123 templated sol–gel route

Mun Teng Soo[a,b], Go Kawamura[b], Hiroyuki Muto[b], Atsunori Matsuda[b], Zainovia Lockman[a], Kuan Yew Cheong[a,*]

[a]*Energy Efficient & Sustainable Semiconductor Research Group (esReG), School of Materials and Mineral Resources Engineering, Engineering Campus, Universiti Sains Malaysia, Seri Ampangan, 14300 Nibong Tebal, Pulau Pinang, Malaysia*

[b]*Department of Electrical and Electronic Information Engineering, Toyohashi University of Technology, 1-1 Hibarigaoka, Tempaku-cho, Toyohashi, Aichi 441-8580, Japan*

Available online 16 October 2012

Abstract

Mesoporous zirconia (ZrO_2) thin films were prepared by dip-coating via Pluronic P123 templated sol–gel route. $ZrOCl_2 \cdot 8\ H_2O$ was used as zirconium (Zr) precursors. Annealing of as-coated ZrO_2 thin films is important in order to stiffen the respective films and to remove the Pluronic P123. The mesoporous structure and crystallite size of ZrO_2 were characterized systematically by field-emission scanning electron microscope (FESEM), both low- and wide-angle X-ray diffraction, thermal analysis technique and Brunauer–Emmett–Teller method. At annealing temperature of 400 °C, amorphous ZrO_2 was transformed into tetragonal phase of ZrO_2 (*t*-ZrO_2). At 450 °C, *t*-ZrO_2 and monoclinic phase of ZrO_2 (*m*-ZrO_2) were obtained. By altering heating rate during annealing, volume fraction of *t*-ZrO_2 and *m*-ZrO_2 was changed. FESEM images showed that disordered mesostructures of ZrO_2 were formed after annealing. The surface area of mesoporous ZrO_2 obtained ranges from 54.33 to 93.39 m^2/g.

Keywords: A. Sol–gel; D. ZrO_2; Mesoporous; Pluronic P123

1. Introduction

Mesoporous materials have attracted widespread interest in different areas of science and technology since after a new family of mesoporous SiO_2 was pioneered by researchers from Waseda University [1] and Mobile Cooperation [2] in the beginning of 1990 s. Their convenient syntheses through different chemical routes, large diversity of framework structures, and novel properties have become a very active area of research for over a decade, and these materials can find vital applications on many frontier areas such as adsorption, catalysis, separation technology, chromatography, and drug delivery.

The unique feature for the synthesis of mesoporous materials is utilization of soft templates such as triblock copolymers or surfactants as a structure-directing agent. As a kind of nonionic surfactants, block copolymer is composed of two or more chemically distinct homopolymer subunits (blocks) linked by covalent bonds. Owing to their mutual repellency, dissimilar blocks tend to segregate into different domains. As confined by chemical connectivity between the blocks, spatial extents of all segregated domains are mostly in a mesoscopic scale. Block copolymer holds excellent self-assembly capability to construct robust mesostructures with rich mesophases. This approach for the synthesis of mesoporous SiO_2-based materials has been extended to transition metal oxides (TMO) [3,4]. Mesoporous TMO are often more difficult to synthesize, often demonstrate low thermal stability, and are usually more susceptible to redox reactions, hydrolysis, or phase transformations.

Mesoporous ZrO_2 is of particular interest in view of their high chemical stability, being potentially applicable as catalyst support [5], adsorbent [6], heavy duty membranes [7] and oxygen sensors [8]. For many of these applications, processing ZrO_2 as a thin film is important. The pioneering

*Corresponding author. Tel.: +604 599 5259, +6012-515-3540; fax: +604 594 1011.
E-mail address: cheong@eng.usm.my (K.Y. Cheong).

0272-8842/$ - see front matter © 2012 Elsevier Ltd and Techna Group S.r.l. All rights reserved.
http://dx.doi.org/10.1016/j.ceramint.2012.10.109

work by the research group of Sanchez [7] represents the preparation of oriented mesostructured ZrO_2 films using diblock copolymer of Brij 58 ($C_{16}H_{33}EO_{10}$) as structuring agent. The oxide presented regularly ordered long-range patterns at the annealing temperature of 60 °C. By increasing the annealing temperature to 300 °C, the pore shapes became ecliptic.

Herein, we report the synthesis of crystallized mesoporous ZrO_2 thin films via sol–gel route, using Pluronic P123 as template. ZrO_2 phase is transformed from amorphous to tetragonal and subsequently to monoclinic as the annealing temperature increases.

2. Experimental procedure

2.1. Chemicals

Zirconium oxychloride octahydrate ($ZrOCl_2 \cdot 8H_2O$, Wako), ethanol (EtOH, Wako) and triblock copolymer Pluronic P123 ($EO_{20}PO_{70}EO_{20}$, Sigma-Aldrich) were used as received. Water was distilled and deionized. The Radio Corporation of America (RCA) cleaning procedure was used to clean silicon (Si) substrates. The procedure requires mixture of H_2O, ammonia solution (NH_3, Wako) and hydrogen peroxide (H_2O_2, Wako) in the volume ratio of 5:1:1.

2.2. Sample preparation

2.2.1. $ZrOCl_2.8H_2O$ as Zr source.

8.22 g of powder $ZrOCl_2 \cdot 8\ H_2O$ was mixed with diluted EtOH (volume ratio of EtOH and H_2O is 4:1) then stirred. A white sol was developed at room temperature. Colloidal particles formed in the sol were mainly hydrated zirconyl oxalate ($ZrOC_2O_4$) peptized by HCl, which was one of the products of the above reaction [9]. Concurrently, 1.36 g Pluronic P123 was dissolved in 20 ml of EtOH by stirring the solution for an hour at room temperature. Then, the dissolved Pluronic P123 was dropped into solution of $ZrOCl_2 \cdot 8H_2O$ while stirring. The solution was stirred for another one hour.

2.2.2. Mesoporous ZrO_2 thin film and powders formation.

The final colloidal sol was used for dip-coating on one side of the Si substrates with an area of $2.0 \times 2.5\ cm^2$ at 24% R.H. The dip-coated samples were dried at room temperature for a day. In order to produce ZrO_2 powders, a certain amount of sol was dried at 60 °C for 3 weeks to allow gelation process. Both the thin films and powders produced were annealed at 400 and 450 °C at heating rate of 0.5 and 5 °C/min respectively for 4 h.

2.3. Characterization methods

Thermogravimetry (TG) and differential thermal analysis (DTA) were carried out in air from room temperature to 800 °C at a rate of 10 °C/min using a Thermo Plus 2 (RIGAKU Thermo Plus TG8120). Structural analyses of ZrO_2 were performed using an X-ray diffractometer (XRD, Rigaku RINT-2000) operated using Cu Kα as X-ray source, voltage at 40 kV, current at 20 mA and scan rate at 0.2°/min with a step of 0.02°. Mesoporous structures of ZrO_2 thin films were analyzed at low-angle (1–5)° XRD range, whereas XRD patterns of ZrO_2 powders were recorded on a range of $2\theta = 15–70°$ for analysis of crystalline phases. The specific surface area of the samples were determined by the Brunauer–Emmett–Teller (BET) method, which was by adsorption/desorption of nitrogen at liquid nitrogen temperature and relative pressures (P/P_0) ranging from 0.1 to 0.25, where P and P_0 are the equilibrium and the saturation pressures of adsorbates at the temperature of adsorption. Before each measurement, the sample was degassed at 300 °C for 30 min. Surface morphology of dip-coated ZrO_2 thin films was observed using a field-emission scanning electron microscope (FESEM, HITACHI High Tech S-4800).

3. Results and discussion

Fig. 1 shows TG–DTA curves for the as-dried gel. The origin of the weight loss is attributed to dehydration and decomposition of oxalate compounds which is represented by two endothermic peaks of DTA curve: (1) at 90 °C – dehydration corresponding to $ZrOC_2O_4.xH_2O \rightarrow ZrOC_2O_4 + xH_2O$; and (2) at 140 °C – decomposition according to $ZrOC_2O_4 + 1/2O_2 \rightarrow ZrO_2 + 2CO_2$ with ~23% weight loss. The release of chlorine takes place during the thermal treatment process. Two exothermic peaks are observed: (1) at 240 °C – corresponds to burning of Pluronic P123 to CO, CO_2 and H_2O with weight loss by 35%; and (2) at 480 °C – indicates crystallization of ZrO_2 with no significant change in TG curve.

Fig. 2 shows the wide-angle XRD patterns of the prepared ZrO_2 powders before and after annealing at different temperatures and heating rates for 4 h. The sample before annealing, for both heating rates, only shows diffraction peaks of crystallized Pluronic P123 [9]. By annealing the sample at 350 °C and above, diffraction peaks related to Pluronic P123 varnished. It shows that Pluronic P123 was completely removed upon annealing at 350 °C, which agrees well with the TG–DTA results. For sample annealed at 350 °C, a broad diffraction peak

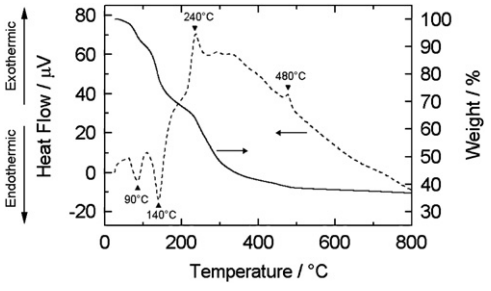

Fig. 1. TG–DTA curves for the combustion process of as-dried gel (after gelation for 60 °C for 96 h).

associated with ZrO_2 is recorded; indicating that the oxide at this stage is amorphous. By increasing the annealing temperature to 400 °C, diffraction peaks of t-ZrO_2 are obtained (ICDD card number 42–1164). Further increases of the annealing temperature to 450 °C, diffraction peaks of m-ZrO_2 were revealed (ICDD card number 37–1484). As the heating rate increases from 0.5 to 5.0 °C/min, crystallinity of the samples decreases.

The mean crystallite size was evaluated from the highest intensity XRD diffraction peak at (100) plane for t-ZrO_2; and (111) plane for m-ZrO_2 using Scherrer formula, $D_{(hkl)}=K\lambda/(\beta_{(hkl)}\cos\theta_{(hkl)})$, where D is the crystallite size, K is the Scherrer constant. K is assumed with value of 1, λ is the wavelength of the radiation (1.5418 Å for Cu Kα radiation), β is the corrected peak width at half-maximum intensity, θ is the corresponding Bragg angle and (hkl) is Miller indices of respective crystal plane of ZrO_2.

The volume fraction of each phase of ZrO_2 was calculated from the empirical equations [10], $x_t=I_{t(100)}/(I_{t(100)}+I_{m(100)}+I_{m(\bar{1}11)})$ and $x_m=1-x_t$, where x_m and x_t represent the volume fraction of t-ZrO_2 and m-ZrO_2, respectively. $I_{(hkl)}$ is the intensity of the selective (hkl) peaks.

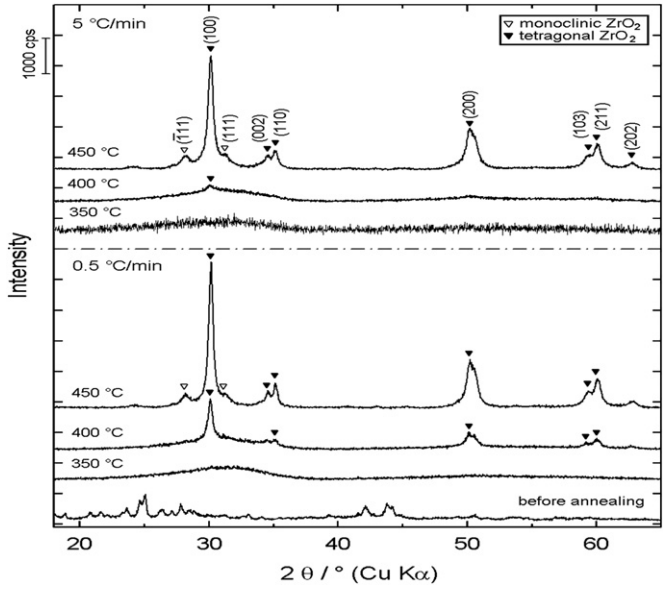

Fig. 2. Wide-angle XRD patterns of the mesoporous ZrO_2 powders before and after annealing at different temperature and heating rate (holding time=4 h).

The phase composition and the crystallite size of as-prepared ZrO_2 powders as a function of annealing temperature are presented in Table 1.

The crystallite size of t-ZrO_2 increases while the content of t-ZrO_2 decreases with the progressing of annealing temperature. By increasing heating rate while maintaining the annealing temperature, crystallite size for both t- and m-ZrO_2 is decreased. At 450 °C, the content of m-ZrO_2 increases as a function of heating rate. In this work, t-ZrO_2 is obtained at annealing temperature as low as 400 °C. It is because the formation of crystallized ZrO_2 is more favorable when $ZrOCl_2\cdot 8H_2O$ is added at room temperature [11]. In fact, the obtained crystallized mesoporous ZrO_2 is important since many applications of mesoporous ZrO_2 such as high-temperature catalytic reactions of fuel cells, require crystallized wall structures because of the high structural strength and electromagnetic properties.

The results of nitrogen adsorption–desorption analysis are shown in Table 1. The results revealed that ZrO_2 exhibits a higher BET surface area after underwent higher annealing temperature and heating rate. The highest BET surface area (93.39 m^2/g) was revealed by sample annealed at 450 °C with heating rate of 5 °C/min. This value is higher than the BET surface area (63.70 m^2/g) of mesoporous ZrO_2 formed by surfactant of poly (methyl methacrylate) (PMMA) as a template [12].

Typical FESEM images of dip-coated mesoporous ZrO_2 thin films, which were formed after annealing, are shown in Fig. 3. The swirling patterns of tubule bundles [Fig. 3(a)] show no preferred orientation and are similar in appearance to those observed by Aksay et al. [13] and Lu et al. [14]. The disordered mesostructures of ZrO_2 thin films formed were in good agreement with the results obtained from low-angle XRD pattern, which no appreciable peaks appeared in the range of 1–5°. Swirling happens when the long axes of the tubules appear to wander over a wide range of slowly curving arrangements, suggesting that the low bending energy of the tubules along their long axes, in which the effect may be understood in terms of a Helfrich bending energy model of tubule surfactant layer [15]. Besides, swirling is consistent with the inability of interface of dip-coated ZrO_2 to impose long-range order on the tubule assembly process [14], in which can be well observed at higher magnification of FESEM images [Fig. 3(b–d)].

Table 1
Phase composition, crystallite size and specific surface area of mesoporous ZrO_2 powders.

Annealing temp. (°C)	Heating rate (°C/min)		Tetragonal phase		Monoclinic phase		BET surface area (m^2/g)
	0.5	5	$D_{(1\,0\,0)}$ (nm)	x_t (%)	$D_{(1\,1\,1)}$ (nm)	x_m (%)	
400	√		17.6	100	–	0	54.33
		√	9.2	100	–	0	68.58
450	√		21.4	82	10.1	18	60.74
		√	18.7	73	8.1	27	93.39

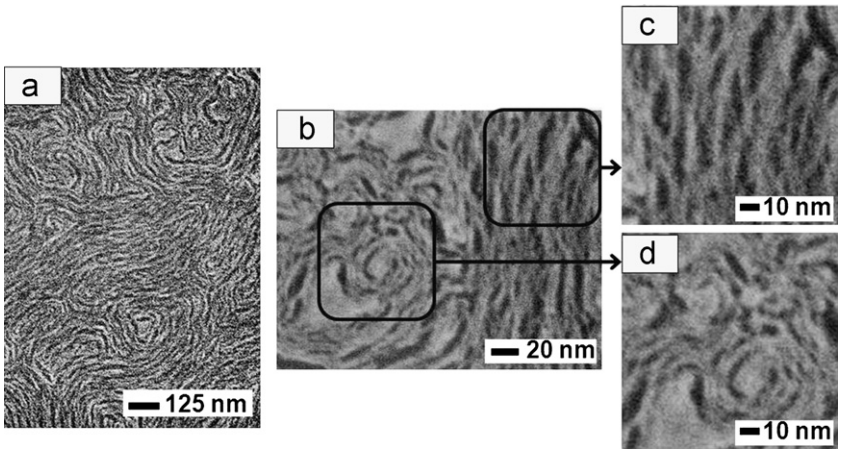

Fig. 3. (a) FESEM image of surface morphology of mesoporous ZrO_2 thin film dip-coated then followed by annealing (450 °C, 4 h, 0.5 °C/min); (b) is the magnified FESEM image of (a); (c) and (d) are the magnified FESEM images at selected regions of (b).

4. Conclusion

In the present study, mesoporous ZrO_2 thin films of disordered mesoporous structure with swirling patterns of tubule bundles were obtained via Pluronic P123 templated sol–gel route. Pluronic P123 surfactant was completely removed from mesoporous ZrO_2 at 350 °C. Different phases of ZrO_2 formed at different annealing temperatures: amorphous ZrO_2 at 350 °C, *t*-ZrO_2 at 400 °C and mixture of *t*-ZrO_2 and *m*-ZrO_2 at 450 °C. At 450 °C with a heating rate of 5 °C/min, mesoporous ZrO_2 obtained possesses the highest BET surface area of 93.39 m^2/g.

Acknowledgments

One of the authors (Mun Teng Soo) would like to thank JENESYS program 2010/2011 and USM fellowship for providing financial support during the study. This project is partly supported by Long Term Research Grant, Ministry of Higher Education Malaysia (2011–2016) with Universiti Teknologi Petronas (Noorhana Yahya) under the OneBaja Project.

References

[1] T. Yanagisawa, T. Shimizu, K. Kuroda, C. Kato, The preparation of alkyltrimethylammonium-kanemite complexes and their conversion to microporous materials, Bulletin of the Chemical Society of Japan 63 (1990) 988–992.
[2] C.T. Kresge, M.E. Leonowicz, W.J. Roth, J.C. Vartuli, J.S. Beck, Ordered mesoporous molecular sieves synthesized by a liquid-crystal template mechanism, Nature 359 (1992) 710–712.
[3] Y. Ma, M. Xing, J. Zhang, B. Tian, F. Chen, Synthesis of well ordered mesoporous Yb, N co-doped TiO_2 with superior visible photocatalytic activity, Microporous and Mesoporous Materials 156 (2012) 145–152.
[4] T. Sreethawong, S. Ngamsinlapasathian, S. Yoshikawa, Crystalline mesoporous Nb_2O_5 nanoparticles synthesized via a surfactant-modified sol–gel process, Materials Letters 78 (2012) 135–138.
[5] P. Doggali, S. Waghmare, S. Rayalu, Y. Teraoka, N. Labhsetwar, Transition metals supported on mesoporous ZrO_2 for the catalytic control of indoor CO and PM emissions, Journal of Molecular Catalysis A: Chemical 347 (2011) 52–59.
[6] H. Zhang, H. Li, W. Li, S. Meng, D. Li, Preparation of TiO_2, CeO_2, and ZrO_2 hierarchically structures in one-pot reactions, Journal of Colloid and Interface Science 333 (2009) 764–770.
[7] E.L. Crepaldi, G.J.A.A. Soler-Illia, D. Grosso, P.A. Albouy, C. Sanchez, Design and post-functionalisation of ordered mesoporous zirconia thin films, Chemical Communications (2001) 1582–1583.
[8] S.A. Ghom, C. Zamani, S. Nazarpour, T. Andreu, J.R. Morante, Oxygen sensing with mesoporous ceria–zirconia solid-solutions, Sensors and Actuators B: Chemical 140 (2009) 216–221.
[9] J. Wang, J. Zhou, Z. Li, Y. He, S. Lin, Q. Liu, M. Zhang, Z. Jiang, Mesoporous mixed metal oxides derived from P123-templated Mg-Al layered double hydroxides, Journal of Solid State Chemistry 183 (2010) 2511–2515.
[10] R.C. Garvie, P.S. Nicholson, Phase analysis in zirconia systems, Journal of the American Ceramic Society 55 (1972) 303–305.
[11] J.L. Blin, R. Flamant, B.L. Su, Synthesis of nanostructured mesoporous zirconia using CTMABr-$ZrOCl_2$.8 H_2O systems: a kinetic study of synthesis mechanisms, International Journal Of Inorganic Materials 3 (2001) 959–972.
[12] G. Duan, C. Zhang, A. Li, X. Yang, L. Lu, X. Wang, Preparation and characterization of mesoporous zirconia made by using a poly (methyl methacrylate) template, Nanoscale Research Letters 3 (2008) 118–122.
[13] I.A. Aksay, M. Trau, S. Manne, I. Honma, N. Yao, L. Zhou, P. Fenter, P.M. Eisenberger, S.M. Gruner, Biomimetic pathways for assembling inorganic thin films, Science 273 (1996) 892–897.
[14] Y. Lu, R. Ganguli, C.A. Drewien, M.T. Anderson, C.J. Brinker, W. Gong, Y. Guo, H. Soyez, B. Dunn, M.H. Huang, Continuous formation of supported cubic and hexagonal mesoporous films by sol–gel dip-coating, Nature 389 (1997) 364–368.
[15] W.Z. Helfrich, Elastic properties of lipid bilayers: theory and possible experiments, Naturforschung 28C (1973) 693–703.